HAL
open science

Evidence of new particle formation within Etna and Stromboli volcanic plumes and its parameterization from airborne in-situ measurements

Maher Sahyoun, Evelyn Freney, Joël Brito, Jonathan Duplissy, Mathieu Gouhier, Aurélie Colomb, Régis Dupuy, Thierry Bourrianne, John Nowak, Chao Yan, et al.

To cite this version:

Maher Sahyoun, Evelyn Freney, Joël Brito, Jonathan Duplissy, Mathieu Gouhier, et al.. Evidence of new particle formation within Etna and Stromboli volcanic plumes and its parameterization from airborne in-situ measurements. Journal of Geophysical Research: Atmospheres, 2019, 10.1029/2018JD028882 . hal-02076923

HAL Id: hal-02076923

https://hal.science/hal-02076923v2

Submitted on 27 Mar 2019

HAL is a multi-disciplinary open access archive for the deposit and dissemination of scientific research documents, whether they are published or not. The documents may come from teaching and research institutions in France or abroad, or from public or private research centers.

L'archive ouverte pluridisciplinaire **HAL**, est destinée au dépôt et à la diffusion de documents scientifiques de niveau recherche, publiés ou non, émanant des établissements d'enseignement et de recherche français ou étrangers, des laboratoires publics ou privés.

Accepted manuscript for publication to the Journal of Geophysical Research, Atmospheres
(manuscript online since 21 March 2019)

Evidence of new particle formation within Etna and Stromboli volcanic plumes and its parameterization from airborne in-situ measurements

Maher Sahyoun[1], Evelyn Freney[1], Joel Brito[1,*], Jonathan Duplissy[2], Mathieu Gouhier[3], Aurélie Colomb[1], Regis Dupuy[1], Thierry Bourianne[4], John B. Nowak[5], Chao Yan[2], Tuukka Petäjä[2], Markku Kulmala[2], Alfons Schwarzenboeck[1], Céline Planche[1], and Karine Sellegri[1]

[1] Laboratoire de Météorologie Physique INSU-CNRS UMR 6016, Université Clermont Auvergne, 63000 Clermont -Ferrand, France

[2] Institute for Atmospheric and Earth System Research/Physics, Faculty of Science, University of Helsinki, P.O. Box 64, 00014 Helsinki, Finland

[3] Laboratoire Magmas et Volcans CNRS, IRD, Observatoire de Physique du Globe de Clermont-Ferrand, Université Clermont Auvergne, 63000 Clermont -Ferrand, France

[4] Center National de Recherches Météorologiques, Météo-France, Toulouse, URA1357, France

[5] Chemistry and Dynamics Branch, NASA Langley Research Center, Hampton, VA 23681, USA

[*] Now at IMT Lille Douai, Université Lille, SAGE, 59000 Lille, France

Corresponding author: Karine Sellegri (k.sellegri@opgc.univ-bpclermont.fr) and Maher Sahyoun (maher.sahyoun@uca.fr).

Key Points:

- New particle formation was evidenced to occur within different volcanic plumes of Etna and Stromboli
- The new particle formation is more pronounced in the free troposphere than in marine boundary layer
- The growth of the newly formed particles to the CCN active size was observed to occur within the volcanic plumes in different rates
- A novel parameterization rate of new particle formation within the Etna's volcanic passive plume was proposed based on the actual measurements

Accepted Article

Please cite this article as doi: 10.1029/2018JD028882

Abstract

Volcanic emissions can significantly affect the Earth's radiation budget by emitting aerosol particles and gas-phase species that can result in the new particle formation (NPF). These particles can scatter solar radiation or modify cloud properties, with consequences on health, weather, and climate. To our knowledge, this is the first dedicated study detailing how gas-phase precursors emitted from volcanic plumes can influence the NPF. A series of airborne measurements were performed around the Etna and Stromboli volcanoes within the framework of the CLerVolc and STRAP projects. The ATR-42 aircraft was equipped with a range of instrumentation allowing the measurement of particle number concentration in diameter range above 2.5 nm, and gaseous species to investigate the aerosol dynamics and the processes governing the NPF and their growth within the volcanic plumes. We demonstrate that NPF occurs within the volcanic plumes in the Free Troposphere (FT) and Boundary Layer (BL). Typically, the NPF events were more pronounced in the FT, where the condensational sink was up to two orders of magnitude smaller and the temperature was ~20°C lower than in the BL. Within the passive volcanic plume, the concentration of sulfur dioxide, sulfuric acid, and $N_{2.5}$ were as high as 92 ppbV, 5.65×10^{8} and 2.4×10^{5} cm^{-3}, respectively. Using these measurements, we propose a new parameterization for NPF rate ($J_{2.5}$) within the passive volcanic plume in the FT. These results can be incorporated into mesoscale models to better assess the impact of the particle formed by natural processes, i.e. volcanic plumes, on climate.

1 Introduction

Volcanic emissions are found to be one of the most abundant natural sources of particles and gases in the atmosphere (Bobrowski et al., 2007; Boulon et al., 2011; Haywood & Boucher, 2000; Oppenheimer et al., 2011; Oppenheimer et al., 2003; Robock, 2000; Tomasi & Lupi, 2016). Volcanos emit a wide range of different gases (SO_2, CO_2, H_2O, H_2S, HF, HBr, …) and particle types (ash and aerosol particles formed from condensable vapors, metals) (Aiuppa et al., 2006; Bobrowski et al., 2007; Mather, 2015; Roberts et al., 2018; Simpson et al., 1999) into the atmosphere. Volcanic aerosols can scatter the solar radiation back to space contributing to a global cooling effect (direct effect) (Albrecht, 1989; Haywood & Boucher, 2000; Robock, 2000), or modify the climatic impacts of clouds (indirect effect) (Mather, 2015 and references within) by acting as cloud condensation nuclei (CCN) (Gassó, 2008; Hobbs et al., 1982; Ilyinskaya et al., 2017; Mather et al., 2003; Mather, 2015) or ice nuclei (IN) (Hoyle et al., 2011). Moreover, volcanic emissions can have significant detrimental effects on human health, the impact of which depends on aerosol physical and chemical properties (Ilyinskaya et al., 2017; Schmidt et al., 2011; Schmidt et al., 2015).

The two main types of volcanic aerosols present in the atmosphere are either primarily emitted or secondarily formed (Mather, 2015; Mather et al., 2003; Petäjä et al., 2012; Roberts et al., 2018; Robock, 2000). The primary volcanic aerosols are mainly volcanic ash and can have diameters ranging from very fine ash (sub-micron) to 2 mm according to classic sedimentology. The very fine ash, which survives proximal sedimentation, usually ranges from sub-micron to a few microns and they result from the fragmentation of the erupting magma into juvenile solid particles injected into a rising column and dispersed in the atmosphere (Allard et al., 2000; Rose & Durant, 2009). The secondary volcanic aerosol particles are produced from the gas-to-particle conversion (secondary formation) process, specifically from the oxidation of SO_2 (Mather et al., 2004; Mather, 2015; Naughton et al., 1975; Schmidt et al., 2011), and this process is not yet well

Accepted Article

characterized within the volcanic plumes. This process is called new particle formation (NPF), where clusters are formed from the gaseous phase as a first step and, later on, grow to larger sizes (> 100 nm) at which they can act as CCN (Hobbs et al., 1982; Mather et al., 2003) or IN (Hoyle et al., 2011) and impact the climate (Kerminen et al., 2012; Kulmala et al., 2001, 2004, 2014; Kulmala & Kerminen, 2008; Kulmala & Laaksonen, 1990; Makkonen et al., 2012). During active eruptions, both primary and secondary particles are present in different atmospheric vertical layers (Ilyinskaya et al., 2017; Mather & Pyle, 2015; Tulet et al., 2017). On the other hand, during passive emissions primary aerosols, with low concentrations, are often limited to the remobilization of accidental lithic (derived from the conduit and crater walls), while emissions of gaseous species may remain significant, likely to contribute to the formation of new particles. It is estimated that ~9 Tg/year of SO_2 is emitted from degassing passive volcanoes worldwide (Allard et al., 1991; Mather et al., 2003; Mather & Pyle, 2015; Pyle & Mather, 2003), being roughly the same order of magnitude of continuously and sporadically eruptive volcanoes (Andres & Kasgnoc, 1998; Carn et al., 2016). Currently, volcanoes contribute to ~10% of the global budget of sulfur emission sources that are dominated by anthropogenic emissions (Allard et al., 1991; Smith et al., 2011). Past studies estimated that aerosol particles with diameters smaller than 0.1 µm contributed a total of 6 to 18% to the total aerosol volume in the passive plume from Etna in Italy (Watson & Oppenheimer, 2000). Whereas in Stromboli (Italy), the contribution of particles in the nucleation and accumulation modes was estimated to be 66% of the total aerosol volume (Allard et al., 2000). Recent studies estimated that global NPF contributes up to 54% of CCN with a large uncertainty range of 38–66% in the present-day atmosphere (Gordon et al., 2017), which is higher than what has been estimated in past studies (Merikanto et al., 2009). In the preindustrial atmosphere simulations, NPF is shown to contribute up to 68% with an even larger range of uncertainty at 45–84% (Gordon et al., 2017). However, a large fraction of the uncertainty on the impact of aerosols on climate stems from the incomplete knowledge of the pre-industrial gas and aerosol concentrations and compositions (Carslaw et al., 2013; Gordon et al., 2016, 2017), therefore, further understanding of such natural processes is crucial.

Sulfuric acid (SA), formed from the oxidation of SO_2 through different channels, is known to be a key species in NPF processes (Kroll et al., 2015; Mauldin et al., 2003; Petäjä et al., 2011; Sipilä et al., 2010; Weber et al., 1996; Weber et al., 2003). Under certain conditions and during mildly eruptive or non-eruptive activity, SA has been observed to be already primarily emitted or secondarily formed in large quantities at some volcanoes (Ilyinskaya et al., 2012; Naughton et al., 1975; Zelenski et al., 2015). Furthermore, the formation of SA and the variation in its concentration in the atmosphere depend strongly on the abundance of SO_2 and the oxidative capacity in the atmosphere (Ilyinskaya et al., 2017; Kroll et al., 2015; Mather, 2015; Schmidt et al., 2012).

While a large number of studies have investigated volcanic emissions through in-situ ground-based and satellite/radar measurements (Carn et al., 2013; Galle et al., 2010; Kantzas & McGonigle, 2008; Mather, 2015; McCormick et al., 2016; McGonigle & Oppenheimer, 2003; McGonigle et al., 2017), airborne in-situ measurements of volcanic emissions remain very scarce (Mauldin et al., 2003; Oppenheimer et al., 2010; Petäjä et al., 2012; Radke, 1982; Rose et al., 2006; Tulet et al., 2017; Vignelles et al., 2016; Weber et al., 2012). The limited number of volcanic plume airborne observations investigating NPF arises from challenges associated with restricted timescales and the impact of temporal and spatial plume's heterogeneities under

Accepted Article

typically harsh environments, besides the costly deployment of highly sophisticated instrumentation aboard an aircraft in such harsh conditions (Delmelle, 2003; Mauldin et al., 2003; Oppenheimer et al., 2003). In that context, the aim of this study is to investigate the aerosol dynamics and the processes governing aerosol formation and growth in different types of volcanic plumes. To the best of our knowledge, this is the first comprehensive dedicated study investigating how gas-phase precursors influence NPF events within different volcanic plumes over Etna and Stromboli using airborne measurements' platforms. Such investigation allows us to characterize the plume spatial extent, its properties, and its intensity and to derive a new parameterization of the rate of NPF. These will permit to further improving the estimation of NPF from natural sources, i.e. volcanic degassing plumes, in models to evaluate more accurately the impact of those particles on climate.

2 Methodology and measurements conditions

2.1 The volcanoes

The airborne measurements were conducted around the Etna and Stromboli volcanoes (Italy). Etna is located on the East coast of Sicily in the Mediterranean Sea (37.75° N, 14.99° E). The vent is located at 3330 m above sea level (a.s.l), typically in the free troposphere (FT). Mount Etna exhibits basaltic eruptions ranging from weakly explosive low-volume activity, such as Stromboli, to more powerful explosive activity leading to fire fountains, which feed columns of scoria, bombs, and ash as jets to heights of tens to hundreds of meters (Calvari et al., 2011). Occasionally, Mount Etna exhibits even more powerful eruptions and produces sub-plinian plumes injecting large amounts of ash and gas, although limited to the troposphere. Inter-eruptive periods are usually characterized by significant emissions of gas, making Etna volcano one of the most important SO_2 emitter (Calvari et al., 2011). During the eruptive activity, the average flux of SO_2 emitted at Etna is typically in the range 10-25 kt/day (Caltabiano et al., 1994), and decreases to 0.6-2 kt/day (Aiuppa et al., 2008; Roberts et al., 2018) during passive emissions. Stromboli is one of the Aeolian Islands in the Mediterranean Sea located in the north coast of Sicily (38.79°N, 15.21°E) and the vent is at 924 m a.s.l., estimated to be in the boundary layer (BL) during our measurements in summer daytime (Seidel et al., 2012). Stromboli volcano is known to exhibit short-lived low-explosive activity with explosions occurring at a time interval of a few tens of minutes on average (Blackburn et al., 1976). The average flux of SO_2 emitted during a standard level of activity lies in the range 0.15-0.6 kt/day (Burton et al., 2008).

During the time of our campaign, Etna was not erupting and only products of passive emissions could be recorded. On the contrary, at Stromboli volcano, the Northeast craters exhibited the typical Strombolian activity with small gas bursts accompanied by the ejection of ballistics every 5-10 min, while the Southwest crater produced less frequent ash-rich explosions. The threshold of the SO_2 flux rate is up to ~5000 t/day for Etna volcano and ~200-300 t/day for Stromboli volcano as reported by the National Institute of Geophysics and Volcanology in Italy for the week between 13 and 20 June 2016, Report. N° 25/2016 on the 21st of June 2016 (National Institute of Geophysics and Volcanology, 2016 a; b).

2.2 Research flights

In 2016, as part of the CLerVolc and STRAP projects (Centre Clermontois de Recherche sur le Volcanisme and Trans-disciplinary collaboration to investigate volcano plumes risks), a series of airborne-based (French research aircraft, ATR-42) measurements were performed

Accepted Article

around Etna and Stromboli volcanoes on the 15th and 16th of June 2016. The ATR-42, operated by the French SAFIRE Facility (Service des Avions Français Instrumentés pour la Recherche en Environnement), intercepted the volcanic plume close to the vent (~2.5 to 5 km) and tracked its evolution for up to 120 km. During this campaign, four flights were conducted: two around Etna (called herein ETNA13 and ETNA14) and two around the Stromboli (called herein STRO14 and STRO15) (Table 1).

Table 1: Summary of ATR-42 flight during STRAP campaign over Etna and Stromboli volcanoes. The date, taking-off and landing time (UTC, UTC=local time –2h) and the maximum and minimum of the longitude, latitude, altitude and the corresponding pressure reached during the flights

Date	**Flight name and number**	Take-off – landing time (UTC)	Latitude range	Longitude range	Altitude range (m) Pressure (hPa) ***FT or BL***
15-Jun-2016	**ETNA13**	10:43:04 – 11:17:49	37.651 – 37.868	14.969 – 15.515	1917-3625 810-659.6 ***FT***
15-Jun-2016	**ETNA14**	14:08:08 – 14:59:58	37.593 – 37.820	15.079 – 15.905	1966-3195 805.3-696 ***FT***
15-Jun-2016	**STRO14**	15:19:53 – 15:54:53	38.652 – 38.852	15.183 – 15.637	715-955 929.6-904.6 ***BL***
16-Jun-2016	**STRO15**	07:38:43 – 08:59:58	38.619 – 39.904	14.408 – 15.449	68-786 997.8-921.2 ***BL***

2.3 Airborne instrumentations

The characterization of the aerosols and gases in the volcanic plumes involved installing a number of instruments in the ATR-42, including: 1) an ultrafine water based Condensation Particle Counters (CPC) (TSI 3788) (Kupc et al., 2013) to measure the total number of particle concentration at a cut-off size > 2.5 nm in diameter; 2) the COndensation PArticle System (COPAS) CPC (Weigel et al., 2009), which is specifically dedicated to aircraft measurements, to measure particles number concentration at size cut-off > 10 nm in diameter; 3) an Optical Particle Counter (Sky OPC, Grimm, # 1.129) to measure the particle size distribution and number concentration in each size bin in the range distributed between 250 nm and 2.5 µm. According to the works of Pirjola et al. (1999), the OPC data in that size range was used to calculate the condensational sink (CS), thus, it represents the lower limit of CS calculated for this study. 4) a UV Fluorescence SO_2 Analyzer Teledyne API (T100 V) to measure the SO_2 concentration with 10 s time resolution; 5) a newly designed ambient ionization inlet (AI) coupled with the Atmospheric Pressure interface – Time Of Flight (AI-APi-ToF) mass spectrometer (MS), developed at Institute for Atmospheric and Earth System Research of the University of Helsinki (Finland) (Junninen et al., 2010), to measure SA concentration (more details about SA calibration is further given in section 2.4).

Accepted Article

This combination of different instruments, all having a time resolution of 1s, covered a wide particle size range (2.5 nm up to ~ 2500 nm in diameter) allowing the measurements of aerosol physical properties and the detection of both nanoparticle nucleation and growth processes. The variables defined from the in-situ measurements of total particle number concentrations (cm^{-3}) together with the SA and SO_2 are summarized in Table 2.

Table 2: Summary of the variables and corresponding instrumentations used during Etna and Stromboli flights on the 15th and 16th of June 2016.

Variable	Name	Unit	Instrument/calculation method	Reference
Total number concentration for particles (N) at diameter > 2.5 nm	$N_{2.5}$	cm^{-3}	Water CPC (TSI 3788)	(Kupc et al., 2013)
N at diameter > 10 nm	N_{10}	cm^{-3}	CPC	(Weigel et al., 2009)
N at diameter > 250 nm	N_{250}	cm^{-3}	Sky OPC GRIMM, # 1.129	Manual (GRIMM, 2008)
N at diameter range between 2.5 and 10 nm	$N_{2.5\text{-}10}$	cm^{-3}	$N_{2.5}$ - N_{10}	Derived in this study
N between 10 and 250 nm	$N_{10\text{-}250}$	cm^{-3}	$N_{10} - N_{250}$	Derived in this study
Sulfuric acid concentration	SA	cm^{-3}	CI-APi-ToF	(Junninen et al., 2010)
Sulfur dioxide mixing ratio	SO_2	ppbV	UV Fluorescence Analyzer Teledyne API	Manual (Model T100U 2011)

Different meteorological variables, such as temperature (T); relative humidity (RH); wind speed (W); dew point temperature; pressure; and turbulence, were also measured aboard the aircraft with a one second time resolution. The statistics and the variation range of the T, RH, and W are shown in Table 3. The time series of the abovementioned meteorological parameters are displayed in Figure S1 (supplementary information) for each flight.

Table 3: Summary of the thermodynamic parameters of the atmosphere measured for the different flights.10th and 90th percentile are given in the square brackets and the median values are given in the second line.

Variable	ETNA13	ETNA14	STRO14	STRO15
T (°C)	[7.4 - 14.4]	[11.5 - 14.7]	[22.9 - 24]	[29.4 - 31.9]
	10.45	12.5	23.5	30.9
RH (%)	[35.2 - 72.6]	[34.2 - 53.3]	[27.6 - 42.5]	[27.6 - 36]
	61.5	42.6	39	30.4
W ($m\ s^{-1}$)	[10.1 - 21.6]	[9 - 19]	[3.8 - 6.6]	[13.5 - 24.5]
	18.2	15.8	5.2	17.9

For flights ETNA13 and ETNA14 that took place in the FT, the temperature was above 5 °C, reaching a maximum of 17.5 °C at ~ 2 km in altitude. In STRO14 and STRO15 that took place in the BL, the temperature was always detected over 20°C at lower altitudes and it was 10 to 20°C higher than the temperatures observed in the FT. The RH did not exceed 62.5% and 82% for flights ETNA13 and ETNA14 and it was even lower in the Stromboli plumes (Figure S.1 and Table 3). The measurements of the cloud droplet probe (CDP) and fast cloud droplet probe

Accepted Article

(FCDP) together with the RH measurements confirm that flights were undertaken in cloud-free conditions.

2.4 SA calibration from AI-APi-ToF

Following the strict aircraft instrumentation regulation concerning chemicals, a new ambient ionization (AI) inlet has been developed for the field campaign avoiding the use of chemical reagents. The AI-APi-ToF is used for the first time on board an aircraft to perform such measurements and provides a 1 s time resolution of a lower estimate of SA concentration. The system utilizes a soft X-ray source (Hamamatsu L9490) to ionize directly the sampled air and increase the overall signal for fast (1 s) measurement. The instrument was also operated in ion mode, like a classical APi-ToF MS mode, where only natural ions are sampled. However, in the ion mode, a long integration time (minimum 10 min) is necessary to obtain the correct signal. The X-ray source was periodically switched ON and OFF (for these flights, 10 seconds ON and 10 seconds OFF), allowing both sampling of natural ions and forced ionized ions. The ATR-42 was flying at an average speed of 360 km/hour; hence, we use the X-ray mode (with one-second resolution) to first identify the different air masses (i.e. inside the plume, outside the plume) and in a second step to analyze the average natural ions spectrum within the volcanic plume. After the flight campaign, a calibration campaign took place during CLOUD11 at the CLOUD chamber similarly to previous CLOUD experiments (Kirkby et al., 2011; Rondo et al., 2016). In the CLOUD chamber, various atmospheric systems were studied with a wide range of species, i.e. SO_2 (0ppb - 2.6ppb), NO_x (0ppb - 33ppb) and organic vapors (alpha-pinene (0ppb - 4.5ppb), isoprene (0ppb - 5ppb), trimethyl-benzene (0ppb - 9ppb)), allowing the characterization of the new flying AI in different atmospheric systems. During this calibration campaign, the new flying AI inlet worked mainly in O_2^- chemical ionization modes, however, when NO_x was at high concentrations in the chamber, NO_3^- ionization could also contribute. Estimates of SA concentration are conducted from the signal that is produced from the ionization of O_2^- ions (HSO_4^-) and NO_3^- (H_2SO_4 NO_3), obtaining a good correlation between well-characterized nitrate APi-ToF MS systems and the instrument used here (supplementary Figure S.3).

2.5 Backward trajectories

The 72 h air mass backward trajectories were calculated first at the vent of the volcano at the beginning of the flight and then at the flight track every 10 minutes along the path of each flight trajectory using the HYSPLIT model (Draxler, 2003; Stein et al., 2016) (Figure S2). According to back-trajectory calculations, the air mass that reached Etna originated mostly from the Atlantic Ocean passing through Spain and the Mediterranean Sea. Similar back-trajectory was observed for STRO14, however, STRO15 back-trajectory suggests an origin crossing above the Saharan desert. During the latter event, a significant aerosol surface area in the background was observed and could be explained by the presence of Saharan dust, in contrast to the other three flights.

2.6 Background and plume conditions

We measured the SO_2 concentration over the Mediterranean in both the FT and BL outside of the volcanic plumes of Etna and Stromboli and the values were ranging from 1.4 to 1.9 ppbV. From the air mass characterization upwind and downwind of Etna (being almost all

Accepted Article

the time in the FT) and Stromboli (in the BL), a background plume threshold value (PTV) of 2 ppbV of SO_2 is used. This threshold value is used to exclude any contributions from ship emissions or other anthropogenic sources, etc. Although the PTV could be considered relatively high when compared to anthropogenic emission levels (usually on average below 1 ppbV) or to other studies (Mauldin et al., 2003), these values were chosen to ensure that our data analysis focused only on measurements within the different volcanic plumes, and to ensure that we do not consider contributions from other sources. The background (outside plume conditions) was also characterized in term of particle concentrations, being defined as median of all the measures (defined in Table 2) when SO_2 < 2 ppbV for Etna (i.e. 1.61 ppbV, 1781 cm^{-3}, 3.2 cm^{-3} and 0.85×10^8 cm^{-3} for SO_2, $N_{2.5}$, N_{250} and SA, respectively) and Stromboli (i.e. 1.26 ppbV, 2100 cm^{-3}, 10.75 cm^{-3} and 0.87×10^8 cm^{-3} for SO_2, $N_{2.5}$, N_{250} and SA, respectively). The SO_2, SA, and particle number concentrations were corrected considering that their backgrounds were subtracted from the plume concentrations in order to quantify the volcanic plume increment. Thus, all the analysis presented in the following sections is under plume conditions.

3 Results and discussion

3.1 Plume spatial extent and total particle number concentrations

The spatial extent (vertical and horizontal) of the different volcanic plumes, represented by the SO_2, is displayed in Figure 1. Once the aircraft arrived at the volcano, a total vertical profile ranging from 0.2 km up to 4 km for both plumes (Figure 1) was performed. The Etna plume appeared to be located at altitudes between 2 and 3.6 km, whereas the Stromboli plume was centered around 0.8 km during STRO14 and as low as 0.2 km during STRO15. We, therefore, assume that both volcanic plumes investigated around Stromboli were in the BL Once the plume vertical distribution was located, a series of horizontal transects took place up to distances of 120 km.

For ETNA13 and ETNA14 and within the plume conditions, the vertical sounding shows that the air mass containing the plume moved towards downwind above 2 km in altitude confirming the presence of the plume in the FT. The median SO_2 concentrations were 13.7 and 13.55 ppbV and reached maximum values at 92.3 and ~ 77 ppbV for ETNA13 and ETNA14, respectively. Since we did not sample the exact center of the plume at the vent where SO_2 should peak, the maximum of SO_2 was observed at altitudes above 3 and ~2.8 km at ~ 13 and 10 km away from the vent for ETNA 13 and 14, respectively (Figure 1; a-b). Subsequently, SO_2 concentrations decreased with distance from the vent and decreased in altitude while travels downwind below 2.8 km (Figure 1; a-b). The plume can still be observed above the altitude of 2.8 km with relatively high SO_2 values above 40 ppbV at ~22 km distant from the vent (Figure 1; a-b).

For STRO14 and STRO15 in BL, the SO_2 median concentrations were 28.33 and 7.3 ppbV and reached the maxima of 83.3 and 78.3 ppbV, respectively (Figure 1; c-d). The median concentration of SO_2 observed in STRO15 is a factor of ~2 less than what was observed in both cases in the FT whereas, in STRO14, the median was a factor of ~2 larger than in the FT. The differences in the median concentrations of the two BL flights can be explained by the relatively low wind speed measured in the case of STRO14 compared to the other flights (Table 3), resulting in the plume being less spread in both horizontal and vertical directions and more concentrated over a shorter range of distance (Figure 1). Since the aircraft missed the core of the plume at the vent, the maximum values were observed at distances ~ 10 to 12 km from the vent

Accepted Article

similarly to Etna plumes and at height of 860 and 120 m (Figure 1; c-d), respectively, indicating a downward transport of the plume. The SO_2 concentration decreases significantly (< 15 ppbV) (Figure 1; d) with distance from the vent.

The concentration of SO_2 measured during all flights is on the same order of magnitude as those observed in previously reported airborne measurement (larger than 10 ppbV) over the Miyaka volcano in the Pacific Ocean in Japan (Mauldin et al., 2003).

Figure1: The plume spatial extent represented by the concentration of SO_2 as a function of altitudes and distance from the volcanic vent for a) ETNA13, b) ETNA14, c) STRO14 and d) STRO15. The dashed lines represent the vents' heights, which are 3.3 and 0.94 km a.s.l for Etna and Stromboli, respectively.

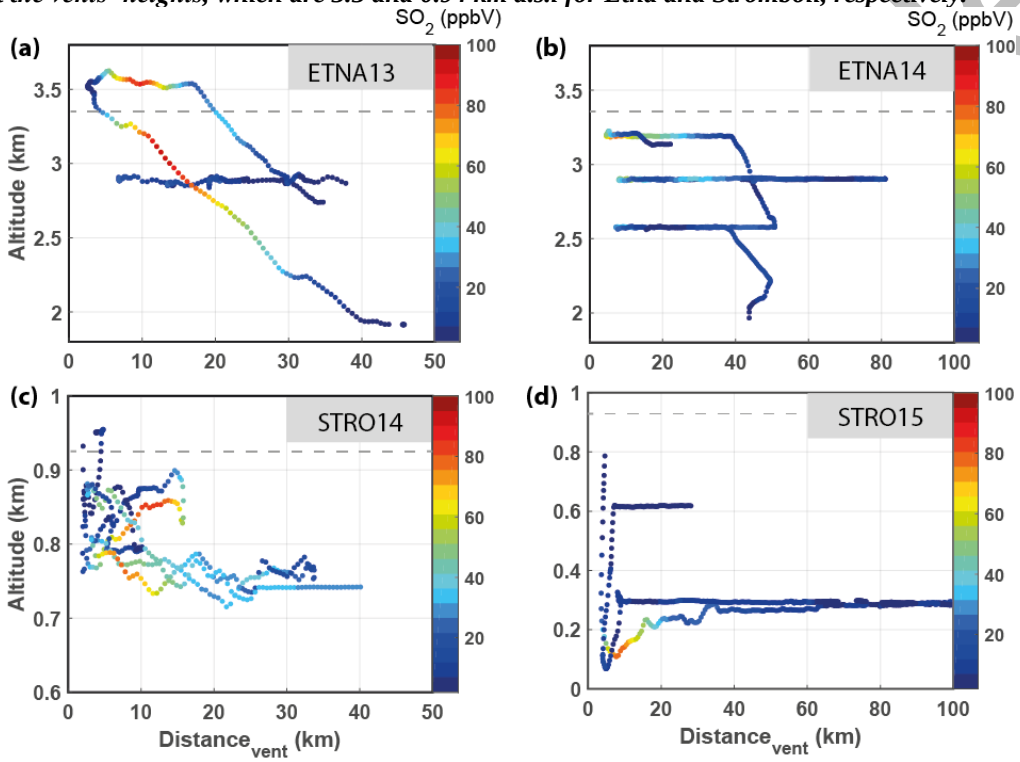

The maps of the aircraft trajectories for the four flights are shown in Figure 2, where the color bar represents the concentration of SO_2, $N_{10\text{-}250}$, and N_{250}. In the FT, $N_{10\text{-}250}$ increased along the plume with median concentrations of ~2500 and 14000 cm^{-3} for ETNA13 and ETNA14, respectively (Table 4). The maximum concentrations of $N_{10\text{-}250}$ were measured to be 34100 cm^{-3} and 25400 cm^{-3} at ~26 and ~47 km distant from the vent. Thus, the $N_{10\text{-}250}$ maxima positions were at ~13 and 37 km farther than the areas where SO_2 maxima were detected (Figure 2; a-b and e-f). The $N_{10\text{-}250}$ increases, on average, from few thousands at ~5 km to few ten thousand at distance > 25 km from the vent, for Etna flights (Figure 2; e-f) and the rate of this increase roughly was ~1500 cm^{-3} per km. This suggests the occurrence of new particle formation and growth along the volcanic plume. For larger particles, the median of N_{250} were 18.8 cm^{-3} and 11 cm^{-3} for flights ETNA13 and ETNA14, respectively (Table 4). During ETNA flights, the N_{250} was relatively high (~70 cm^{-3}) close to the vent (~ 7 km), but decreased significantly (< 20 cm^{-3}) with the plume dilution (Figure 2;i- j and Figure S4). This is opposite to what was measured for smaller particles ($N_{10\text{-}250}$) where a higher concentration was detected along the volcanic plume in the FT especially in the diluted plume (> 25 km) of both Etna flights (Figure 2; e-f).

Figure2: Maps of the trajectory of the different flights in the FT and BL. The color-coded bars represent the corrected (background subtracted) observation of SO_2 (a-d), N_{10-250} (e-h) and N_{250} (i-l).

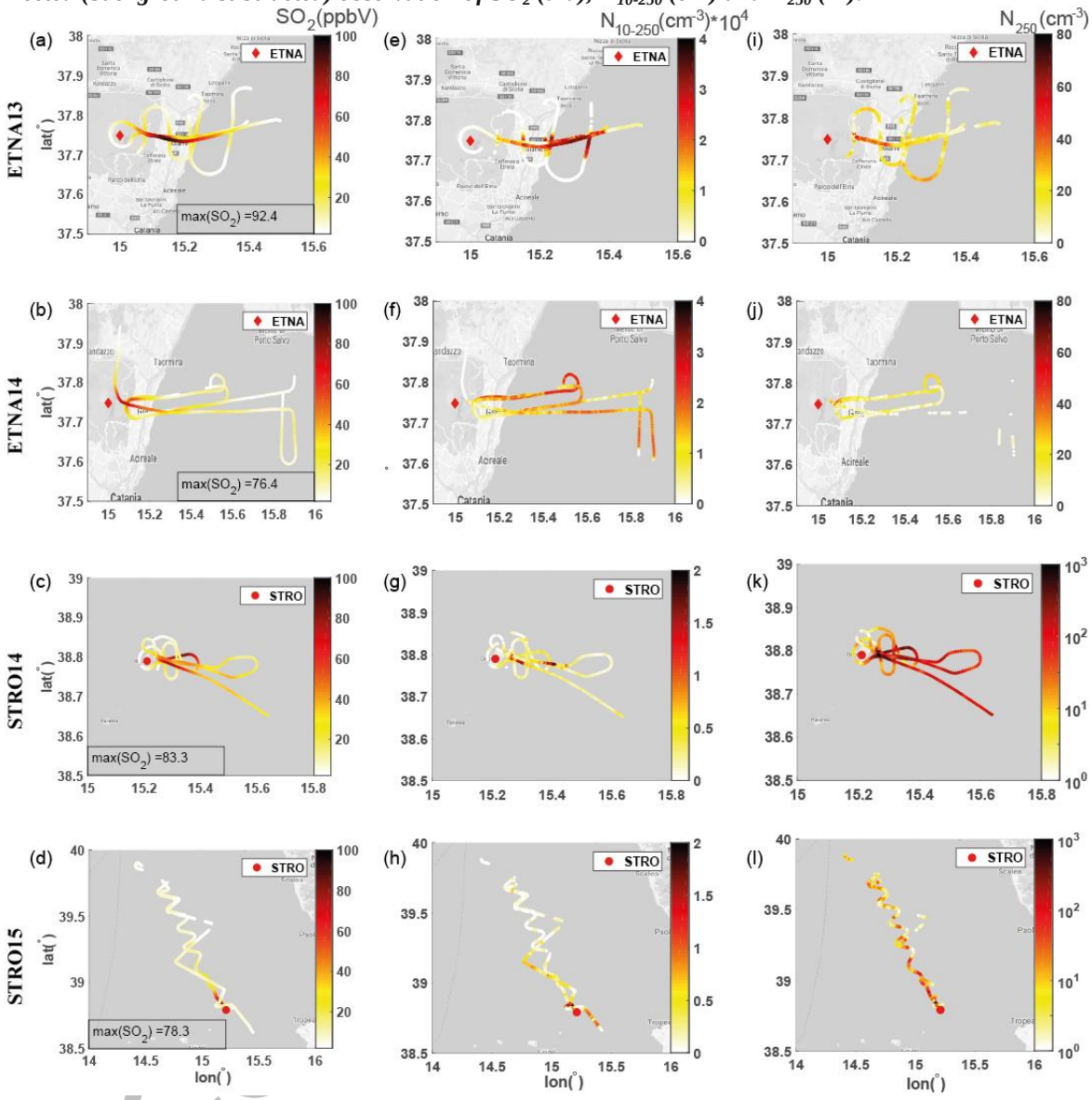

Considering that the volcanic emissions in ETNA13 and ETNA14 during the time of the campaign were passive, the presence of large particles can mainly be interpreted as the rapid growth of freshly nucleated particles. This hypothesis is confirmed by the correlation between N_{100}, N_{250}, and N_{10} (Figure S5; a, c). We do not exclude that some fraction of these particles may also be due to the presence of very fine primary particles (accidental lithic) remobilized from the previous deposits within the conduit and volcanic crater walls, but we estimate that their contribution to the total aerosol concentration was minimal in our observation in the FT (Figure S5; a, c).

For STRO14 and STRO15, N_{10-250} was observed with relatively large values (> 10^4 cm^{-3}) close to the vent at ~ 4 km, respectively, and then decreased significantly with distance from the vent (Figure 2; g-h), except the area where N_{10-250} peaks at ~12 km distant from the vent for STRO14 (Figure 2; g). The N_{10-250} maxima were 18809 cm^{-3} and 19700 cm^{-3} at ~12 km and ~7 km for STRO14 and STRO15, respectively, where SO_2 was also observed to be relatively large

(> 60 ppbV). This is in contrast to what we observed for Etna plumes, where the N_{10-250} maxima were located farther downwind (i.e. at 26 and 47 km distant from the vent. The median of N_{10-250} concentrations were 2470 cm^{-3} and 1300 cm^{-3} for both Stromboli flights, i.e. close to the N_{10-250} median concentration measured within the ETNA13 but one order of magnitude less than the median N_{10-250} observed for ETNA14.

Table 4: Summary of the number concentrations (cm^{-3}) of particles at different diameter ranges, SA concentration and the CS rate (s^{-1}) measured during the different flights. 25th and 75th percentiles are in the first line in square brackets and medians are in the second line.

VARIABLE	ETNA13	ETNA14	Stro14	Stro15
$N_{2.5-10}$ (cm^{-3})	[0.99 2.4]*10^4 4.2*10^3	[0.41 1.1]*10^5 7.7*10^4	[0.4 1.3] *10^3 638.5	[171 741] 351
N_{10-250} (cm^{-3})	[0.053 1.9]*10^4 2.51*10^3	[0.7 1.81]*10^4 1.4*10^4	[1.1 3.7]*10^3 2.47*10^3	[428 3.1*10^3] 1.3*10^3
N_{250} (cm^{-3})	[11.2 27.6] 18.8	[5.4 16.8] 11	[16.6 150.5] 68.2	[2.5 72.5] 35
SA (cm^{-3})	[0.85 3.9]*10^8 2.9*10^8	[3.35 3.94]*10^8 3.71*10^8	[2.34 2.94]*10^8 2.67*10^8	[3 3.5]*10^8 3.3*10^8
SO_2 (ppbV)	[6.2 25] 13.7	[7.5 21.6] 13.55	[13 37.6] 28.3	[4.5 9.6] 7.3
CS (s^{-1})	[0.5 3.1]*10^{-4} 1.6*10^{-4}	[0 2.3]*10^{-4} 6*10^{-5}	[0.65 9.8]*10^{-3} 4.2*10^{-3}	[0 4.5]*10^{-3} 8.1*10^{-4}

For BL flights, the N_{250} is observed to be high peaking at 1081 and 718.5 cm^{-3} near the vent ^{3}at ~ 7 and 5.2 km and continue possessing high values downwind along the plume dilution reaching 225 cm^{-3} at 23 km distant from the vent (Figure 2; c-d and k-l). In general, the N_{250} in the BL was observed to be higher than in the FT; the medians are factor of 3 to 6 higher in the FT (Table 4) and the absolute values are two orders of magnitude higher close to the vent and all along the plume dilution (Figure 2; i-l). The presence of those large particles in the BL flights is due to the quick growth of newly formed particles at distances less than 10 km close to the vent (Figure S5; b, d blue points marked by a blue circle) and distant from the vent with a different growth rate (Figure S5; b, d light blue to red points marked by a red circle). Besides, close to the vent in STRO14, there is likely a contribution from very fine juvenile ash ejected during the short explosions at Stromboli (Figure S5; b, d; blue points marked by a green circle), which can be a significant contribution to the total aerosol surface area. Moreover, in STRO15 and based on the backward trajectory analysis, there may also be a contribution from the Saharan dust particles that arrive from North Africa to the measured areas (Figure S2). Due to the lack of aerosol composition measurements, we are unable to accurately quantify these contributions. The higher concentrations of large particles during BL flights would eventually contribute to a larger aerosol surface area along the volcanic plumes compared to FT flights within Etna's volcanic plumes.

In the following section, we will investigate the NPF and their potential growth processes occurring within these two different volcanic plumes.

Accepted Article

3.2 Observation of new particle formation within different volcanic plumes

The total number concentrations of particles between 2.5 nm and 10 nm ($N_{2.5\text{-}10}$), the SA concentrations (defined in Table 2) and CS are illustrated in Figure 3. For FT flights, $N_{2.5\text{-}10}$ concentrations were observed above the detection limit throughout both plumes and up to ~45 km away from the vent. For both Etna flights, the $N_{2.5\text{-}10}$ is a factor of ~2 to 10 larger than the $N_{10\text{-}250}$ concentrations. This suggests that nucleation is taking place within the volcanic passive plume in the FT (Figure 2; e-f, and Figure 3; a-b). Linked to this nucleation process occurring along the volcanic passive plume, a high concentration of SA (> 10^8 cm^{-3}) is continuously observed; being produced from the oxidation of SO_2 (Figure 3; e-f). The maximum of $N_{2.5\text{-}10}$ was observed where the SA concentration was greater than $2x10^8$ cm^{-3}, and the CS was minimum (Figure 3; a-b, e-f, i-j).

During BL flights, NPF was also observed, but high concentrations of $N_{2.5\text{-}10}$ were mostly located close to the vent (< 10 km). However, the median concentration of $N_{2.5\text{-}10}$ was up to 2 orders of magnitude less than in the FT flights. These show the evidence that new particles were formed within the different volcanic plumes close to the vent (~ 3km) for both Etna and Stromboli volcanic plumes with different rates, but also far from the vent (> 35 km) along the dilution of the passive plume from Etna in the FT. The higher concentrations of large particles (> 250 nm) in the BL result in a higher CS than in the FT (Figure 1; i-l, Figure 2; i-l, and Figure S4 and S5). Interestingly, the concentration of SO_2 and SA were observed to be in comparable ranges for both volcanic plumes (Figures 1, 2; a-d and 3; e-h), and therefore do not explain solely the differences in magnitude in NPF between the FT and BL. Therefore, the greater CS together with the higher temperature, observed in the BL flights than in the FT flights, are likely to explain the weaker NPF events within the volcanic plumes in the BL (Table 2 and 4, Figure 3, and Figure S1).

Moreover, the growth behavior of the newly formed particles was distinct between ETNA and STRO plumes (Figure S4 and S5). The Correlations between newly formed particles and larger particles are observed along the volcanic plumes in both the FT and the BL (Figure S4 and S5). The growth rate, represented by the different slopes, varied according to the distance from the vent and the SO_2 abundance (Figure S4 and S5). The growth is observed to increase at areas closer to the vent (< 20 km) than at farther areas than 20 km (Figure S4 and S5). Since SA was abundant during all flights (Figure 3; e-h), it likely played a key role in NPF and growth processes (CCN active size) within the volcanic plumes in FT and BL. It should be stressed that in the absence of the chemical analysis of the grown particles in our observation, we do not exclude the contribution of other condensable vapors to the growth of the freshly formed particles in the volcanic plumes. The growth of the newly formed particles to CCN active diameters illustrates that those particles within the volcanic plumes can contribute to cloud formation, thus, impacting the weather and climate. Such an observation might be useful for further modeling studies to investigate the contribution of NPF to the CCN and their impact on climate and reduce the associated uncertainty.

Figure3: Observed $N_{2.5\text{-}10}$ (a-d), SA (e-h) and CS(i-l) along the flight trajectory within the plumes of Etna and Stromboli. Gaps visible in the different trajectories are attributed to instrumental data nonavailability.

Accepted Article

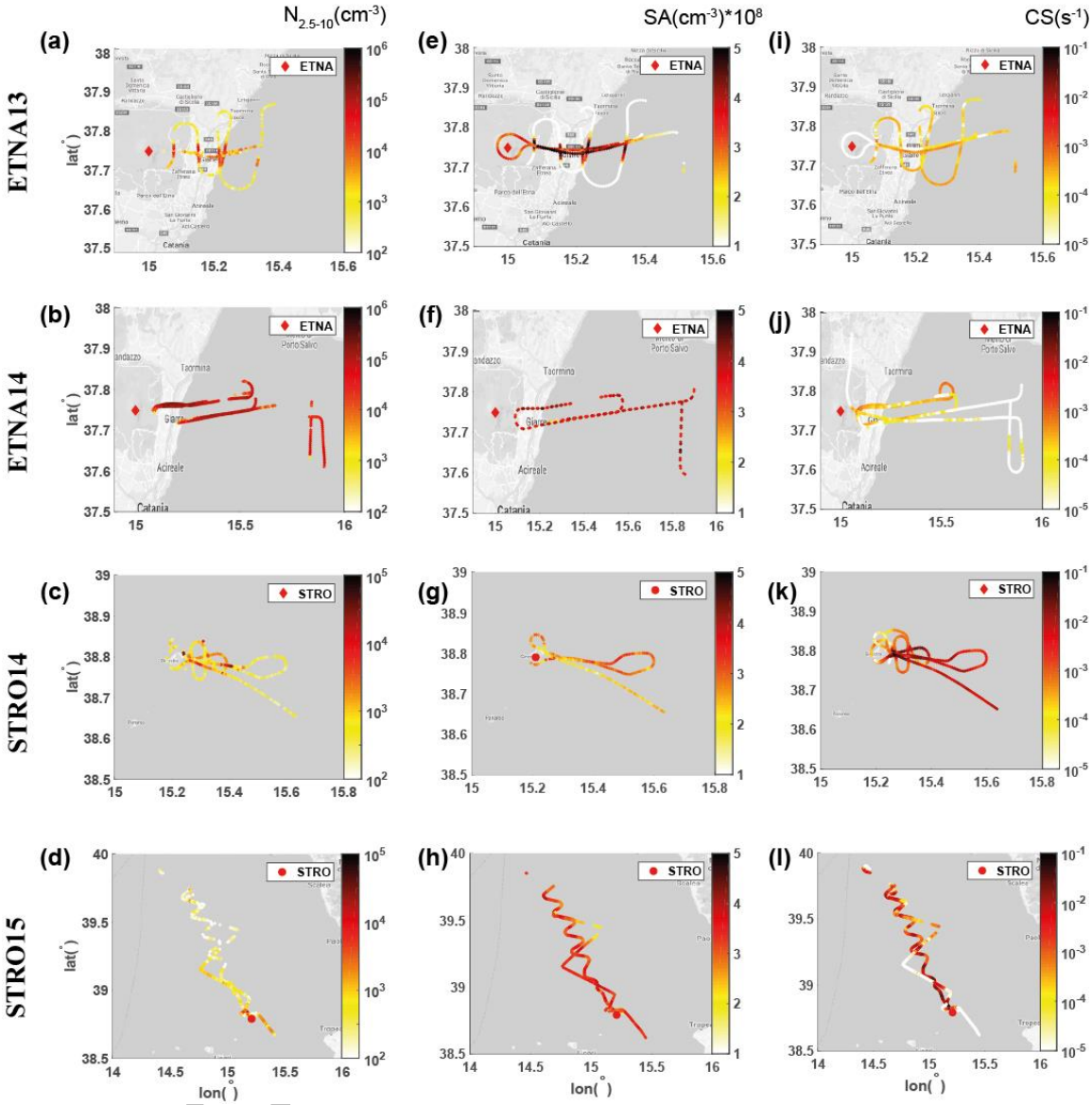

The volcanic SA was also observed to be abundant in other volcanic plumes of Etna (Roberts et al., 2018) and in other locations, i.e. Miyaka and Kilauea (Kroll et al., 2015; Mauldin et al., 2003). This abundance was found to be variable according to several factors related to SO_2 concentrations and its oxidation rates, meteorological variables, i.e. wind speed, temperature and relative humidity (Kroll et al., 2015; Roberts et al., 2018). In comparison to other studies, the SA observed within ETNA and STRO flights were almost of the same order of magnitude to what has been reported in the Pacific BL volcanic plume from the Miyaka volcano (Mauldin et al., 2003; Weber et al., 2003). On the other hand, the median of $N_{2.5\text{-}10}$ measured in Stromboli plumes in MBL is almost one order of magnitude larger than the upper limit (100 cm^{-3}) reported in the MBL volcanic plume in the Pacific from Miyaka volcano for the similar size range (3-4 and 3-8 nm) (Mauldin et al., 2003). The presence of large aerosol surface area may explain our observation of relatively low $N_{2.5\text{-}10}$ in the BL, in comparison to $N_{2.5\text{-}10}$ observed in the FT. Similarly, in the Pacific BL volcanic plume from Miyaka volcano (Mauldin et al., 2003), the

presence of pre-existing particles is given by the authors as an explanation of the low N_{3-4} and N_{3-8} concentrations.

The spatial distributions of the plumes were analyzed in more details, through plume latitudinal transects at different distances from the vent in both ETNA13 and STRO15 (Figure 4).

Figure4: ***$N_{2.5-10}$ and N_{10} as a function of distance from the center of the plume for ETNA13 (a and b) and STRO15 (d, e, g, and h). The plots (g) and (h) are similar to (d) and (e) but with a larger horizontal extent from the center of the plume in STRO15. The considered transects are highlighted by the corresponding colors in the right panel (c for Etna and f for Stromboli).***

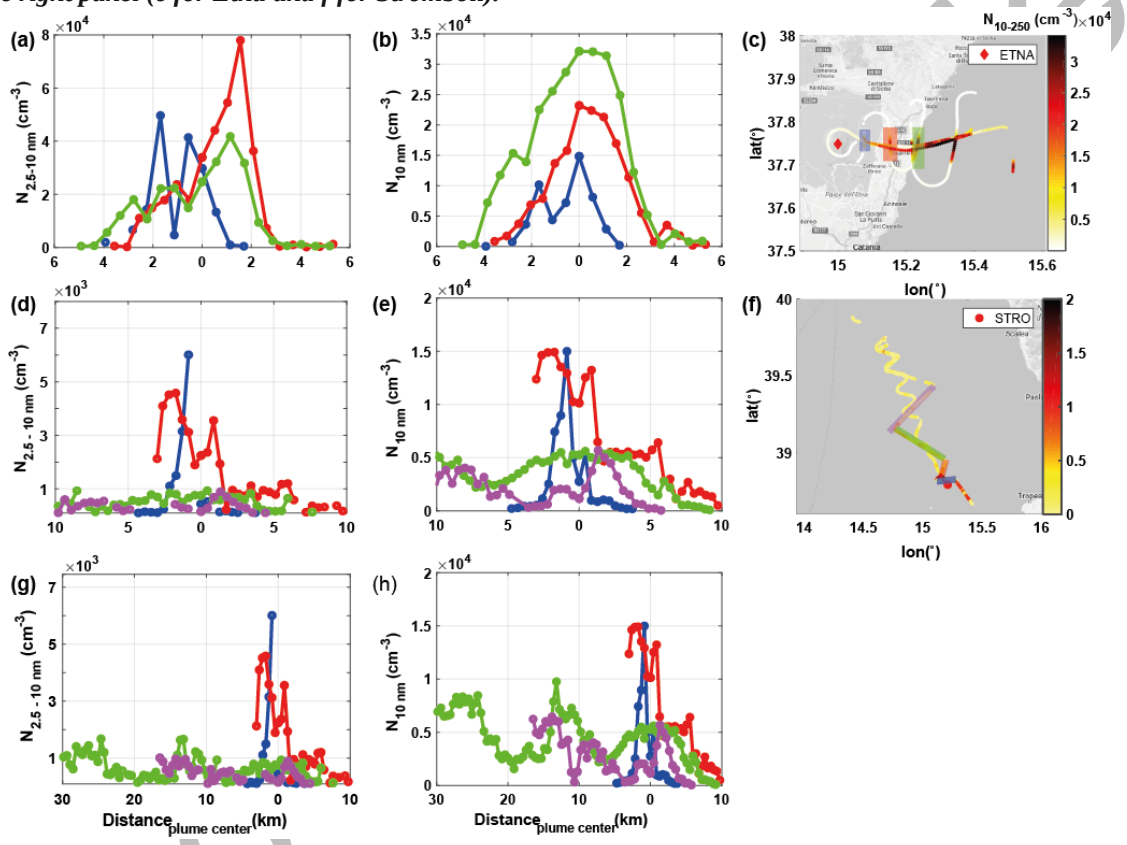

In each transect (highlighted in blue, red, green and purple in Figure 4; c, f), we determined the center of the plume by the peak of SO_2 (not shown). The plume widths are of the order of 6-8 km for the two transects nearest to the volcanoes (respectively at ~7 and ~10 km from the vent) for both volcanoes (Figure 4; a, b, d, and e). Further downwind, the STRO15 plume width increases to about 30 km at ~ 80 km distant from the vent (Figure 4; g, h). For the ETNA13 and STRO15 flights, their corresponding $N_{2.5-10}$ maxima were not observed at the center of the plume, but at the edges of the plumes (Figure 4; a, d). Conversely, N_{10} possesses the maxima exactly at the center of the plume in the FT (Figure 4; b), whereas in the BL it was also shifted to the plume's border (Figure 4; e). These results support that the presence of large CS at the center of the plume is likely to explain the peaks shifting of $N_{2.5-10}$ (and N_{10} in the BL), inhibiting the nucleation process (despite SA continuously produced by oxidation of SO_2) compared to more favorable conditions at the plume periphery, where the CS is lower. The relationships between the particle concentrations in the smallest size bin and their gas-phase precursors, as a function of the distance from the volcanoes' vents, are further investigated in the following section.

3.3 Derivation of new particle formation parameterization

The data from the in-situ measurements are used to derive a parameterization that can be useful to describe the rate of NPF as a function of SA concentration under natural conditions. One hypothesis in our derivation of the nucleation rate is that losses of newly formed particles due to coagulation are negligible compared to the strength of the nucleation rate. Thus, we believe that our calculation is the lower estimate of the nucleation rate within the volcanic plumes. Nucleation rates were derived when the nucleation mode particle concentrations ($N_{2.5}$) was increasing with processing time (*t*) for several periods and locations, where NPF was observed to occur (Figure 5, a and d; areas are highlighted by blue). The parameter *t* is the time needed for an air mass originating from the vent to reach the point where it was sampled by the aircraft. This time is estimated here by integrating the wind speed along the plume with the distance from the vent as following:

$$t = \frac{x_0}{\bar{V}_x} + \sum_{i=x_0+1}^{i=L} \frac{\Delta x}{V(i)}$$

x_0 is the distance between the closest point from the flight trajectory inside the volcanic plume and the vent, $\bar{V}_x$ is the mean wind speed of all the trajectory points, L is the farthest point from the vent of flight trajectory within the plume, Δx is the distance traveled by the aircraft from the source point (vent) and $V(i)$ is the corresponding wind speed of each point of the flight trajectory. Since the nucleation events were found to be more pronounced in the FT than in the BL, a nucleation rate could only be calculated along the plumes in the FT, and hence the parameterization is solely based on Etna emissions. We plot the particle concentration increase as a function of the processing time by taking into account the dilution of the plume with transport within the plume. It is important to note that the volcanic passive plume at Etna contains a low concentration of CO (upper limit was 110 ppbV), a typical gas used as a dilution factor (*di*). Therefore during this study, SO_2 is used as a dilution factor, while its concentration is strongly enhanced in the plume and has a typical tropospheric average lifetime of 1-2 days (Beirle et al., 2014), and thus, is partially consumed during the plume evolution. A dilution factor, defined as the SO_2 concentration normalized by its maximum value for each flight, was hence applied to the particle concentration to calculate normalized particle number concentrations. Figure 5 (b, c, e and f) shows the normalized $N_{2.5}$ concentrations as a function of *t* to evaluate the correlation between these two variables. For ETNA13, we divided the flight into two periods: a) from 10:40 to 10:55 when the aircraft only crossed the plume at different distances from the vent, and b) from 11:00 to 11:15 when the aircraft was flying within the center of the plume. For ETNA14, we furthermore chose two periods where the NPF events were observed to occur at two different altitudes in the FT: c) from 14:28 to 14:32 at ~2.8 km and d) from 14:34 to 14:38 ~3.3 km. In period (a), we calculated the mean value of each particle peak, each corresponding to a single processing time (Figure 5; b). The fit of those points against *t* was linear (Figure 5, b), yielding a slope of 11 cm^{-3} s^{-1}. In period (b), the function between normalized $N_{2.5}$ concentrations and the *t* was exponential (Figure 5; c). The rate of NPF ($j_{2.5}$) for each nucleation event is then the derivative of each of the above-mentioned regressions for the two periods for flight ETNA13. Similarly to the period (b), the regression for the two chosen periods for flight ETNA14 was found to be exponential as well (Figure 5; e and f).

Figure5: Time series of the total number concentration of particles at different cut-off sizes for ETNA13 (a) and ETNA14 (d) with the $N_{2.5}$ versus processing time with their fitting regressions at different periods (b) 10:40

Accepted Article

to 10:55 UTC, (c) from 11:00 to 11:15 UTC for flight ETNA13, (e) from 14:28 to 14:33 UTC and (f) from 14:34 to 14:38 UTC

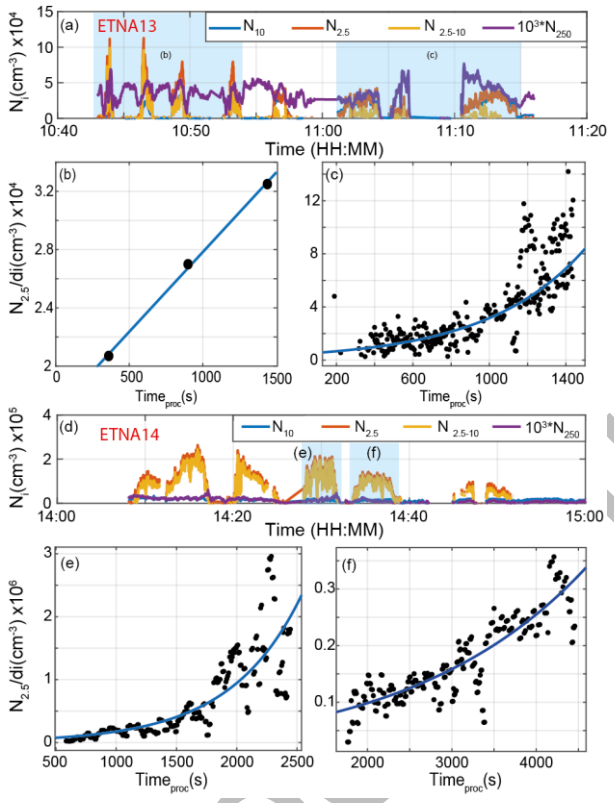

Table 5 shows all the derived relationships between the normalized $N_{2.5}$ vs. t with their fitting parameters A and B to estimate the nucleation rate $j_{2.5}$. The relationship has either a linear form as in a period (a) (illustrated in Figure 5; b) or an exponential form as in periods (b, c, and d) (illustrated in Figure 5; c, e, and f):

$$j_{2.5} = d(N_{2.5}/di)/dt = A\,e^{Bt} \quad (1)$$

Table 5: Summary of the derivative of the correlation between the normalized $N_{2.5}$ and corresponding processing time shown in Figure 5 (b, c, e, and f) with their fitting parameters for the different periods in the case of ETNA13 and ETNA14 in the free troposphere. The confidence bounds for all regressions were 95%.

	ETNA13		**ETNA14**	
Period	(a) 10:40 to 10:55	(b) 11:00 to 11:15	(c) 14:28 to 14:32	(d) 14:34 to 14:38
Regression of $N_{2.5}$/di vs t	$11 \times t + 17000$	$4505 \times e^{1.95\times10^{-3}\times t}$	$32280 \times e^{1.7\times10^{-3}\times t}$	$37990 \times e^{4.8\times10^{-4}\times t}$
$j_{2.5}$ = d($N_{2.5}$/di)/dt	11	$9 \times e^{1.95\times10^{-3}\times t}$	$55 \times e^{1.7\times10^{-3}\times t}$	$18 \times e^{4.8\times10^{-4}\times t}$
R^2	0.99	0.8814	0.9123	0.8124
Adjusted R^2	0.98	0.881	0.9119	0.8116

Figure 6 shows all estimated $j_{2.5}$ for all Etna points in the FT versus SA together with their averages (black dots) every 0.25×10^8 cm^{-3}. We derive the parameterization of NPF rate $J_{2.5}$ by

fitting the averages of all estimated $j_{2.5}$ to the corresponding SA using the bi-squares method, with 95% confidence bounds, of the simple power model that has the form:

$$J_{2.5} = K[SA]^P \quad (2)$$

where pre-factor K and exponent P are the fitting parameters of the power function and, estimated to be 1.844×10^{-8} s^{-1} and 1.12 (95% confidence interval 0.76 and 1.47), respectively. The exponent P, found in the current study, is closer to 1 (associated with activation-type nucleation) (Kulmala et al., 2006) rather than kinetic-type nucleation (2) (McMurry & Friedlander, 1979), in agreement with what has previously been hypothesized (Kuang et al., 2008; Sihto et al., 2006). According to our derivation and by substituting the values of K, P and the medians of SA from Table 4 for ETNA13 and ETNA14, the average $J_{2.5}$ is 68.6±39.9 and 59.23±29.8 cm^{-3} s^{-1}, respectively, and equal to 63.23±34.8 cm^{-3} s^{-1} for all ETNA points.

Figure6: The calculated $J_{2.5}$ versus SA for the different periods of all ETNA flights in the free troposphere. The black dots and the associated error bars on the panel (a) are the mean and the standard deviation of the $J_{2.5}$ obtained within 0.25×10^8 cm^{-3} SA equal bins. The black dots in panel (b) are the mean $J_{2.5}$ as a function of SA for the specific SA range defined by the light red shaded area on the panel (a) when SA is smaller than 4.6×10^8 cm^{-3}. In the panel (b), the correlation between $J_{2.5}$ and SA is a power fit (red line), which represents the parameterization of the new particle formation within the volcanic plume $J_{2.5} = 1.844\times10^{-8}[SA]^{1.12}$.

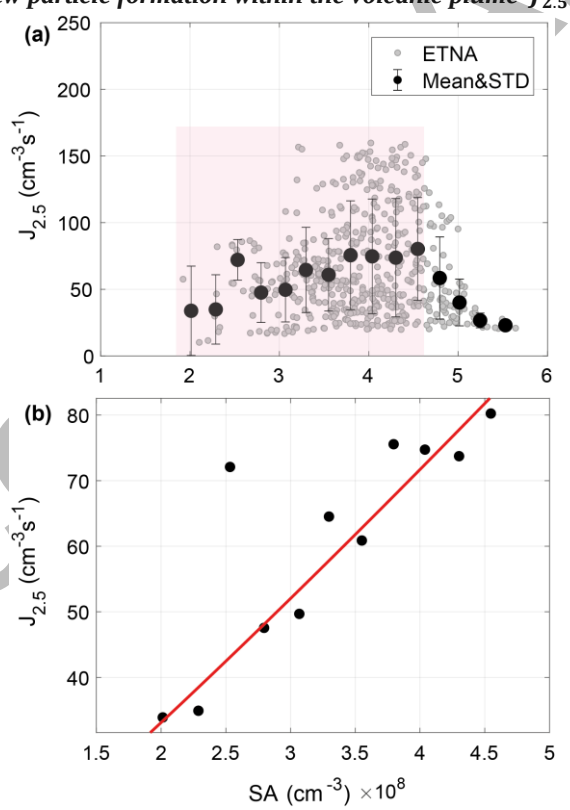

In our derivation, the coagulation process was neglected in comparison to the strength of the nucleation process, therefore, the $J_{2.5}$ values derived here are considered as the lower limits of nucleation. Based on Quantum Chemistry-normalized Classical Nucleation Theory (QC-CNT) and CLOUD measurements presented in Duplissy et al. (2016), the nucleation of new particles is minimized when SA was below 10^8 cm^{-3} at temperatures above 10°C. This indicates that the SA background (up to 0.85×10^8 cm^{-3}), which was subtracted from the data, would not have a significant impact on our derivation of the NPF rate. Moreover, this parameterization is valid

when SA is less than 4.6×10^8 cm^{-3} (Figure 6; a). For values of SA larger than 4.6×10^8, $J_{2.5}$ has been observed to significantly decrease with increasing SA (Figure 6; a) due to the large CS estimated at distances close to the vent (less than 5 km) or in the center of the plume, where growth is observed to be stronger than NPF. For the SA values greater than 4.6×10^8 cm^{-3}, we believe that the approximation of negligible coagulation is no longer valid. In comparison to more cleaner environments, our lower limits estimations of $J_{2.5}$ are one to almost 2 orders of magnitude higher than what has been previously measured in Hyytiälä (Finland) during the QUEST2 campaign in 2003 by Sihto et al. (2006) for J_3. The formation rate $J_{2.5}$ is a factor of ~2.5 to 4 higher than the upper limit of J_1 found for the same campaign (Kuang et al., 2008; Sihto et al., 2006). These suggest a quicker occurrence of NPF within the harsh environment of the volcanic passive plume in comparison to what has been found in other cleaner environments (Sihto et al., 2006). In comparison to the controlled CLOUD3 and CLOUD5 experiments of SA-water binary particle formation for the same range of SA, our estimation of $J_{2.5}$ is comparable or an order of magnitude higher than the J resulted from the exposure to different beams in the CLOUD chamber (Figure 9 in Duplissy et al., 2016). This may indicate that condensable vapors other than SA could be contributing to the NPF events. Indeed, Kirkby et al. (2011) showed that ~100 pptV of ammonia may increase nucleation up to a factor of 1000 more than what binary SA-water nucleation can produce. However, in the absence of chemical characterization, our observations were not able to confirm the contribution of the other species than sulfuric acid to the NPF process. Our estimation of $J_{2.5}$ is found to be more than one order of magnitude higher than what was estimated, on average, within the aged volcanic plume that reached the puy de Dôme station, Massif Central (France) (4.76 ± 2.63 cm^{-3} s^{-1}) in May 2010 from the Eyjafjallajökull eruption event (Boulon et al., 2011). This is expected since the plume in that study traveled several thousands of kilometers before reaching the station, whereas our measurements are occurring directly within the passive plume. This indicates how efficient the volcanic passive plume can be especially in the free troposphere where new particle formation is favored. Substituting the average estimated value of SA ($3.67 \pm 0.78 \times 10^7$ molecules cm^{-3}) from Boulon et al. (2011) in our parameterization formula (equation 2) would give an NPF rate of 5.02 cm^{-3} s^{-1}, which is close to the average nucleation rate actually calculated from the Eyjafjallajökull plume (Boulon et al., 2011). This indicates that our parameterization would be able to reproduce the average nucleation rate J_2 estimated for the volcanic plumes even with SA less than 10^8 cm^{-3} at locations far from the eruptive point. Yet, the binary homogeneous H_2SO_4-H_2O nucleation scheme (BHNS) (Kulmala et al., 1998) and activation nucleation (Sihto et al., 2006) have been used in a previous modeling study that investigated the impact of volcanic aerosols on climate (Schmidt et al., 2012). The BHNS was found to underestimate the climatic impact of freshly formed particles in the volcanic degassing plumes (Boulon et al., 2011; Schmidt et al., 2012). Therefore, our current analysis together with the parameterization can effectively contribute to better understand and quantify the climatic impacts of aerosol nucleation and their evolution within volcanic plumes near the volcanic source and in the diluted volcanic plumes.

4 Conclusions

This study presents a comprehensive investigation of new particle formation and growth within volcanic plumes located in the FT and in the BL. This was conducted by performing airborne in-situ measurements within the plumes of Etna and Stromboli, Italy.

Accepted Article

We evidenced the occurrence of new particle formation and growth of these newly formed particles within the different plumes from Etna in the FT and Stromboli in the BL. In the FT, the NPF events were measured in the volcanic passive plume near the vent with a rapid growth rate, and continue to occur efficiently along the plume at distances farther than 35 km. The rapid growth of the newly formed particles was observed close to the vent results in a relatively high number concentration of large particles (N_{250} > 55 cm^{-3}) and hence a relatively significant CS (up to 10^{-2} s^{-1} in absolute value). However, the concentration of these large particles is diluted with distance, and therefore the threshold ratio between the condensable gases and the condensational sink is overcome by the presence of sufficient SA from SO_2 oxidation to allow for further nucleation events. In the BL, the NPF events were also observed close to the vent of the volcano and with smaller concentrations of ultrafine particles than in the FT. The SO_2 fluxes at Stromboli were reported to be weak (0.15-0.6 kt/day, (Burton et al., 2008)), but they remain comparable with those emitted at Etna during passive degassing (0.6-2 kt/day, (Aiuppa et al., 2008; Roberts et al., 2018)). This has been supported by our observations, where we found that SO_2 and SA concentrations were relatively comparable and the differences in their values in different volcanic plumes of Etna (being passive) and Stromboli are small. Thus, these small differences in SO_2 and SA concentrations between Etna and Stromboli do not explain solely the NPF being more dominant in Etna (in the FT) than in Stromboli (in the BL). Therefore, the occurrence of the NPF events in the different volcanic plumes seems to be largely influenced by the presence of large particles leading to large CS at the very proximity to the vent. Thus, the weaker NPF events in the BL is a result of a larger aerosol surface along the plume, where CS was up to 2 orders of magnitude higher than in the FT, and with temperatures reaching 23 and 30 °C in both BL flights, which is up to 20°C higher than in the FT. This detailed analysis of the growth of freshly nucleated particles to the CCN sizes (Figure S4 and S5) is beneficial for further modeling studies to investigate the contribution of NPF to the CCN and their impact on climate.

To the authors' knowledge, this is the first dedicated study that addresses the relationship between the newly formed nanoparticles and their gas-phase precursors in the vicinity of different volcanic plumes over Etna and Stromboli. The in-situ airborne measurements performed as part of this study within the ETNA passive plume were used to derive NPF rate parameterizations $J_{2.5}$ that can eventually be incorporated into models. The NPF rate was an exponential function of the processing time in most of the observed individual nucleation events along the flight trajectories and implicitly includes the information about the plume's dilution. The NPF rate parameterization was a power law function of SA, with an exponent value of 1.12, which is accepted within the range of what has previously been reported (Kuang et al., 2008; Sihto et al., 2006). The latter exponent value implies that the nucleation within the studied plumes is a natural process that is a mixture of both activation (Kulmala et al., 2006) and kinetic (McMurry & Friedlander, 1979) nucleation modes, but more close to the activation nucleation mode. We believe that our calculation is the lower estimate of the nucleation rate within the volcanic plume since the losses due to coagulation are neglected compared to the strength of the nucleation rate. This new parameterization has a simple formula and is able to reproduce the same average nucleation rate for the volcanic plumes observed in locations thousands of kilometers distant from the erupted event (Boulon et al., 2011). Therefore, this parametrization of particle formation rate, based on actual measurements, is a more representative of the nucleation process occurred under largely uncharacterized volcanic degassing plumes conditions. The new parametrization should further be tested in mesoscale models coupled with chemistry transport scheme and compared with pre-existing parametrizations for new particle formation

Accepted Article

within volcanic plumes. It should be noted that although SA is the key factor for the NPF events within the different volcanic plumes, we cannot exclude that condensable vapors other than SA, e.g. halogens and organic vapors, could be participating to the nucleation and growth processes in the FT and BL, and the latter should be investigated by deeper chemical characterization in future studies. Finally, this study contributes to better understand and quantify the natural process of the gas to particle conversion within volcanic plumes, and how this process with the resulted aerosol concentrations evolves temporally and spatially in the atmosphere aiming to reduce the uncertainty of the aerosol's impact on climate.

Acknowledgments

The authors would like to thank the three anonymous reviewers for their constructive comments and suggestions, which contributed significantly to the improvement of the article.

The data of these measurements are possessed by the STRAP program and available on STRAP website http://osur.univ-reunion.fr/recherche/strap/database/. The lead author and this work are funded by the ClerVolc project - Programme 1 "Detection and characterization of volcanic plumes and ash clouds" funded by the French government 'Laboratory of Excellence' initiative, ClerVolc contribution number 311. The authors would like to extend a special thanks to the pilots and flight crew from SAFIRE for all their enthusiasm and support during the measurement campaign aboard the ATR-42 aircraft. We would also like to thank Dr. Douglas R. Worsnop, Vice President/Director in Aerodyne Incorporation, for the information to develop the ambient ionization inlet to be used with the APi-ToF instrument onboard.

References

Aiuppa, A., Federico, C., Giudice, G., Gurrieri, S., Liuzzo, M., Shinohara, H., et al. (2006). Rates of carbon dioxide plume degassing from Mount Etna volcano. *Journal of Geophysical Research*, *111*(B9), B09207. https://doi.org/10.1029/2006JB004307

Aiuppa, A., Giudice, G., Gurrieri, S., Liuzzo, M., Burton, M., Caltabiano, T., et al. (2008). Total volatile flux from Mount Etna. *Journal of Geophysical Reseach*, *35*, 12809–12819. https://doi.org/10.1029/2008GL035871

Albrecht, B. A. (1989). Aerosols, Cloud Microphysics, and Fractional Cloudiness. *Science*, *245*(4923), 1227–1230. https://doi.org/10.1126/science.245.4923.1227

Allard, P., Carbonnelle, J., Dajlevic, D., Bronec, J. L., Morel, P., Robe, M. C., et al. (1991). Eruptive and diffuse emissions of CO2 from Mount Etna. *Nature*, *351*(6325), 387–391. https://doi.org/10.1038/351387a0

Allard, P., Aiuppa, A., Loyer, H., Carrot, F., Gaudry, A., Pinte, G., et al. (2000). Acid gas and metal emission rates during long-lived basalt degassing at Stromboli volcano. *Geophysical Research Letters*, *27*(8), 1207–1210. https://doi.org/10.1029/1999GL008413

Andres, R. J., & Kasgnoc, a. D. (1998). A time-averaged inventory of subaerial volcanic sulfur emissions. *J. Geophys. Res.*, *103*(D19), 25251. https://doi.org/10.1029/98JD02091

Beirle, S., Hörmann, C., Vries, M. P. De, Dörner, S., Kern, C., & Wagner, T. (2014). Estimating the volcanic emission rate and atmospheric lifetime of SO 2 from space : a case study for Kılauea volcano , Hawai ' i, 8309–8322. https://doi.org/10.5194/acp-14-8309-2014

Blackburn, E. A., Wilson, L., & Sparks, R. J. (1976). Mechanisms and dynamics of strombolian activity. *Journal of the Geological Society*, *132*, 429–440.

Bobrowski, N., Glasow, R. Von, Aiuppa, A., Inguaggiato, S., Louban, I., & Ibrahim, O. W. (2007). Reactive halogen chemistry in volcanic plumes, *112*(November 2006), 1–17. https://doi.org/10.1029/2006JD007206

Boulon, J., Sellegri, K., Hervo, M., & Laj, P. (2011). Observations of nucleation of new particles in a volcanic plume. *Proceedings of the National Academy of Sciences of the United States of America*, *108*(30), 12223–6. https://doi.org/10.1073/pnas.1104923108

Burton, M. R., Caltabiano, T., Murè, F., Salerno, G., & Randazzo, D. (2008). SO2 flux from Stromboli during the 2007 eruption: Results from the FLAME network and traverse measurements. *Journal of Volcanology and Geothermal Research*, *182*, 214–220. https://doi.org/10.1016/j.jvolgeores.2008.11.025

Caltabiano, T., Romano, R., & Budetta, G. (1994). SOz flux measurements at Mount Etna (Sicily). *Journal of*

Accepted Article

Geophysical Reseach, *99*(94), 12809–12819.

Calvari, S., Salerno, G. G., Spampinato, L., Gouhier, M., Spina, A. La, Pecora, E., et al. (2011). An unloading foam model to constrain Etna ' s 11 – 13 January 2011 lava fountaining episode. *Journal of Geophysical Reseach*, *116*(January), 1–18. https://doi.org/10.1029/2011JB008407

Carn, S. A., Krotkov, N. A., Yang, K., & Krueger, A. J. (2013). Measuring global volcanic degassing with the Ozone Monitoring Instrument (OMI). *Geological Society, London, Special Publications*, *380*(1), 229–257. https://doi.org/10.1144/SP380.12

Carn, S. A., Clarisse, L., & Prata, A. J. (2016). Multi-decadal satellite measurements of global volcanic degassing. *Journal of Volcanology and Geothermal Research*, *311*, 99–134. https://doi.org/10.1016/J.JVOLGEORES.2016.01.002

Carslaw, K. S., Lee, L. A., Reddington, C. L., Pringle, K. J., Rap, A., Forster, P. M., et al. (2013). Large contribution of natural aerosols to uncertainty in indirect forcing. *Nature*, *503*(7474), 67–71. https://doi.org/10.1038/nature12674

Delmelle, P. (2003). Environmental impacts of tropospheric volcanic gas plumes. *Geological Society, London, Special Publications*, *213*(1), 381–399. https://doi.org/10.1144/GSL.SP.2003.213.01.23

Draxler, R. R. (2003). Evaluation of an Ensemble Dispersion Calculation. *Journal of Applied Meteorology*, *42*(2), 308–317. https://doi.org/https://doi.org/10.1175/1520-0450(2003)042<0308:EOAEDC>2.0.CO;2

Duplissy, J., Merikanto, J., Franchin, A., Tsagkogeorgas, G., Kangasluoma, J., Wimmer, D., et al. (2016). Effect of ions on sulfuric acid-water binary particle formation: 2. Experimental data and comparison with QC-normalized classical nucleation theory. *Journal of Geophysical Research: Atmospheres*, *121*(4), 1752–1775. https://doi.org/10.1002/2015JD023539

Galle, B., Johansson, M., Rivera, C., Zhang, Y., Kihlman, M., Kern, C., et al. (2010). Network for Observation of Volcanic and Atmospheric Change (NOVAC)—A global network for volcanic gas monitoring: Network layout and instrument description. *Journal of Geophysical Research*, *115*(D5), D05304. https://doi.org/10.1029/2009JD011823

Gassó, S. (2008). Satellite observations of the impact of weak volcanic activity on marine clouds. *Journal of Geophysical Research*, *113*(D14), D14S19. https://doi.org/10.1029/2007JD009106

Gordon, H., Sengupta, K., Rap, A., Duplissy, J., Frege, C., Williamson, C., et al. (2016). Reduced anthropogenic aerosol radiative forcing caused by biogenic new particle formation. *PNAS*, *113*(43), 12053–12058. https://doi.org/10.1073/pnas.1602360113

Gordon, H., Kirkby, J., Baltensperger, U., Bianchi, F., Breitenlechner, M., Curtius, J., et al. (2017). Causes and importance of new particle formation in the present-day and preindustrial atmospheres. *Journal of Geophysical Research: Atmospheres*, *122*(16), 8739–8760. https://doi.org/10.1002/2017JD026844

GRIMM. (2008). Specification for Model 1.129 Sky-Optical Particle Counter (full version). *Users' Manual*, 1–44. Retrieved from www.grimm-aerosol.com

Haywood, J., & Boucher, O. (2000). Estimates of the direct and indirect radiative forcing due to tropospheric aerosols: A review. *Reviews of Geophysics*, *38*(4), 513–543. https://doi.org/10.1029/1999RG000078

Hobbs, P. V., Tuell, J. P., Hegg, D. A., Radke, L. F., & Eltgroth, M. W. (1982). Particles and gases in the emissions from the 1980–1981 volcanic eruptions of Mt. St. Helens. *Journal of Geophysical Research*, *87*(C13), 11062. https://doi.org/10.1029/JC087iC13p11062

Hoyle, C. R., Pinti, V., Welti, A., Zobrist, B., Marcolli, C., Luo, B., et al. (2011). Ice nucleation properties of volcanic ash from Eyjafjallajökull. *Atmos. Chem. Phys. Atmospheric Chemistry and Physics*, *11*, 9911–9926. https://doi.org/10.5194/acp-11-9911-2011

Ilyinskaya, E., Martin, R. S., & Oppenheimer, C. (2012). Aerosol formation in basaltic lava fountaining: Eyjafjallajökull volcano, Iceland. *Journal of Geophysical Research: Atmospheres*, *117*(D20). https://doi.org/10.1029/2011JD016811

Ilyinskaya, E., Schmidt, A., Mather, T. A., Pope, F. D., Witham, C., Baxter, P., et al. (2017). Understanding the environmental impacts of large fissure eruptions: Aerosol and gas emissions from the 2014-2015 Holuhraun eruption (Iceland). *Earth and Planetary Science Letters*, *472*, 309–322. https://doi.org/10.1016/j.epsl.2017.05.025

Junninen, H., Ehn, M., Petäjä, T., Luosujärvi, L., Kotiaho, T., Kostiainen, R., et al. (2010). A high-resolution mass spectrometer to measure atmospheric ion composition. *Atmospheric Measurement Techniques*, *3*(4), 1039–1053. https://doi.org/10.5194/amt-3-1039-2010

Kantzas, E. P., & McGonigle, A. J. S. (2008). Ground Based Ultraviolet Remote Sensing of Volcanic Gas Plumes. *Sensors (Basel, Switzerland)*, *8*(3), 1559–1574. https://doi.org/10.3390/s8031559

Kerminen, V.-M., Paramonov, M., Anttila, T., Riipinen, I., Fountoukis, C., Korhonen, H., et al. (2012). Cloud

Accepted Article

condensation nuclei production associated with atmospheric nucleation: a synthesis based on existing literature and new results. *Atmospheric Chemistry and Physics*, *12*(24), 12037–12059. https://doi.org/10.5194/acp-12-12037-2012

Kirkby, J., Curtius, J., Almeida, J., Dunne, E., Duplissy, J., Ehrhart, S., et al. (2011). Role of sulphuric acid, ammonia and galactic cosmic rays in atmospheric aerosol nucleation. *Nature*, *476*(7361), 429–433. https://doi.org/10.1038/nature10343

Kroll, J. H., Cross, E. S., Hunter, J. F., Pai, S., Wallace, L. M. M., Croteau, P. L., et al. (2015). Atmospheric evolution of sulfur emissions from KIlauea: Real-time measurements of oxidation, dilution, and neutralization within a volcanic plume. *Environmental Science and Technology*, *49*(7), 4129–4137. https://doi.org/10.1021/es506119x

Kuang, C., McMurry, P. H., McCormick, A. V., & Eisele, F. L. (2008). Dependence of nucleation rates on sulfuric acid vapor concentration in diverse atmospheric locations. *Journal of Geophysical Research Atmospheres*, *113*(10), 1–9. https://doi.org/10.1029/2007JD009253

Kulmala, M., & Kerminen, V.-M. (2008). On the formation and growth of atmospheric nanoparticles. *Atmospheric Research*, *90*(2–4), 132–150. https://doi.org/10.1016/J.ATMOSRES.2008.01.005

Kulmala, M., & Laaksonen, A. (1990). Binary nucleation of water–sulfuric acid system: Comparison of classical theories with different H 2 SO 4 saturation vapor pressures. *The Journal of Chemical Physics*, *93*(1), 696–701. https://doi.org/10.1063/1.459519

Kulmala, M., Laaksonen, A., & Pirjola, L. (1998). Parameterizations for sulfuric acid/water nucleation rates. *Journal of Geophysical Research Atmospheres*, *103*(D7), 8301–8307. https://doi.org/10.1029/97JD03718

Kulmala, M., Dal Maso, M., Mäkelä, J. M., Pirjola, L., Väkevä, M., Aalto, P., et al. (2001). On the formation, growth and composition of nucleation mode particles. *Tellus, Series B: Chemical and Physical Meteorology*, *53*(4), 479–490. https://doi.org/10.1034/j.1600-0889.2001.d01-33.x

Kulmala, M., Vehkamäki, H., Petäjä, T., Dal Maso, M., Lauri, A., Kerminen, V. M., et al. (2004). Formation and growth rates of ultrafine atmospheric particles: A review of observations. *Journal of Aerosol Science*, *35*(2), 143–176. https://doi.org/10.1016/j.jaerosci.2003.10.003

Kulmala, M., Lehtinen, K. E. J., & Laaksonen, A. (2006). Cluster activation theory as an explanation of the linear dependence between formation rate of 3 nm particles and sulphuric acid concentration. *Atmos. Chem. Phys. Atmospheric Chemistry and Physics*, *6*, 787–793. Retrieved from www.atmos-chem-phys.net/6/787/2006/

Kulmala, M., Petäjä, T., Ehn, M., Thornton, J., Sipilä, M., Worsnop, D. R., & Kerminen, V.-M. (2014). Chemistry of Atmospheric Nucleation: On the Recent Advances on Precursor Characterization and Atmospheric Cluster Composition in Connection with Atmospheric New Particle Formation. *Annual Review of Physical Chemistry*, *65*(1), 21–37. https://doi.org/10.1146/annurev-physchem-040412-110014

Kupc, A., Bischof, O., Tritscher, T., Beeston, M., Krinke, T., & Wagner, P. E. (2013). Laboratory Characterization of a New Nano-Water- Based CPC 3788 and Performance Comparison to an Ultrafine Butanol-Based CPC 3776 Laboratory Characterization of a New Nano-Water-Based CPC 3788 and Performance Comparison to an Ultrafine Butanol-Based CPC 3776. *Aerosol Science and Technology*, *47*(47). https://doi.org/10.1080/02786826.2012.738317

Makkonen, R., Asmi, A., Kerminen, V.-M., Boy, M., Arneth, A., Hari, P., & Kulmala, M. (2012). Air pollution control and decreasing new particle formation lead to strong climate warming. *Atmospheric Chemistry and Physics*, *12*(3), 1515–1524. https://doi.org/10.5194/acp-12-1515-2012

Mather, T. A. (2015). Volcanoes and the environment: Lessons for understanding Earth's past and future from studies of present-day volcanic emissions. *Journal of Volcanology and Geothermal Research*, *304*, 160–179. https://doi.org/10.1016/j.jvolgeores.2015.08.016

Mather, T. A., & Pyle, D. M. (2015). Volcanic emissions: short-term perturbations, long-term consequences and global environmental change. In A. Schmidt, K. E. Fristad, & L. T. Elkins-Tanton (Eds.), *Volcanism and Global Environmental Change*. Cambridge: Cambridge University Press. https://doi.org/10.1017/CBO9781107415683

Mather, T. A., Pyle, D. M., & Oppenheimer, C. (2003). Tropospheric volcanic aerosol (pp. 189–212). American Geophysical Union. https://doi.org/10.1029/139GM12

Mather, T. A., Oppenheimer, C., Allen, A. G., & McGonigle, A. J. S. (2004). Aerosol chemistry of emissions from three contrasting volcanoes in Italy. *Atmospheric Environment*, *38*(33), 5637–5649. https://doi.org/10.1016/J.ATMOSENV.2004.06.017

Mauldin, R. L., Cantrell, C. A., Zondlo, M., Kosciuch, E., Eisele, F. L., Chen, G., et al. (2003). Highlights of OH , H2SO4 , and methane sulfonic acid measurements made aboard the NASA P-3B during Transport and Chemical Evolution over the Pacific, *108*, 1–13. https://doi.org/10.1029/2003JD003410

Accepted Article

McCormick, K. B., Edmonds, M., & Biggs, J. (2016). Observing eruptions of gas-rich compressible magmas from space. *Nature Communications*, *7*, 13744. https://doi.org/10.1038/ncomms13744

McGonigle, A. J. S., & Oppenheimer, C. (2003). Optical sensing of volcanic gas and aerosol emissions. *Geological Society Special Publication*, *213*(January), 149–168. https://doi.org/10.1144/GSL.SP.2003.213.01.09

McGonigle, A. J. S., Pering, T. D., Wilkes, T. C., Tamburello, G., D'Aleo, R., Bitetto, M., et al. (2017). Ultraviolet Imaging of Volcanic Plumes: A New Paradigm in Volcanology. *Geosciences*, *7*(3), 68. https://doi.org/10.3390/geosciences7030068

McMurry, P. H., & Friedlander, S. K. (1979). New particle formation in the presence of an aerosol. *Atmospheric Environment (1967)*, *13*(12), 1635–1651. https://doi.org/10.1016/0004-6981(79)90322-6

Merikanto, J., Spracklen, D. V, Mann, G. W., Pickering, S. J., & Carslaw, K. S. (2009). Impact of nucleation on global CCN. *Atmos. Chem. Phys. Atmospheric Chemistry and Physics*, *9*, 8601–8616. Retrieved from www.atmos-chem-phys.net/9/8601/2009/

Model T100U Trace Level Sulfur Dioxide Analyzer. (2011). *Users' Manual*, (August).

National Institute of Geophysics and Volcanology. (2016). *Bollettino settimanale sul monitoraggio vulcanico, geochimico e sismico del vulcano Etna, Rep. N° 25/2016*. Retrieved from http://www.ct.ingv.it/en/rapporti/multidisciplinari.html?view=docman&start=195

Naughton, J. J., Lewis, V., Thomas, D., & Finlayson, J. B. (1975). Fume compositions found at various stages of activity at Kilauea Volcano, Hawaii. *Journal of Geophysical Research*, *80*(21), 2963–2966. https://doi.org/10.1029/JC080i021p02963

Oppenheimer, C., Pyle, D. M. (David M. ., & Barclay, J. (Jenni). (2003). *Volcanic degassing*. Geological Society. Retrieved from https://books.google.fr/books?hl=en&lr=&id=zsPoH-aCJqwC&oi=fnd&pg=PA1&dq=does+degassing+volcanic+plume+contain+volcanic+ash&ots=z92tWRuquM&sig=iOxAN0eZXyUqa_MsyuUjcdrQKxM#v=onepage&q=does degassing volcanic plume contain volcanic ash&f=false

Oppenheimer, C., Kyle, P., Eisele, F., Crawford, J., Huey, G., Tanner, D., et al. (2010). Atmospheric chemistry of an Antarctic volcanic plume. *Journal of Geophysical Research Atmospheres*, *115*(4), 1–15. https://doi.org/10.1029/2009JD011910

Oppenheimer, C., Scaillet, B., & Martin, R. S. (2011). Sulfur Degassing From Volcanoes: Source Conditions, Surveillance, Plume Chemistry and Earth System Impacts. *Reviews in Mineralogy and Geochemistry*, *73*(1), 363–421. https://doi.org/10.2138/rmg.2011.73.13

Petäjä, T., Sipilä, M., Paasonen, P., Nieminen, T., Kurtén, T., Ortega, I. K., et al. (2011). Experimental Observation of Strongly Bound Dimers of Sulfuric Acid: Application to Nucleation in the Atmosphere. *Physical Review Letters*, *106*(22), 228302. https://doi.org/10.1103/PhysRevLett.106.228302

Petäjä, T., Laakso, L., Grönholm, T., Launiainen, S., Evele-Peltoniemi, I., Virkkula, A., et al. (2012). In-situ observations of Eyjafjallajökull ash particles by hot-air balloon. *Atmospheric Environment*, *48*, 104–112. https://doi.org/10.1016/J.ATMOSENV.2011.08.046

Pirjola, L., Markku, K., Martin, W., Albrecht, B., Frank, S., & Eckhard, O. (1999). Formation of sulphuric acid aerosols and cloud condensation nuclie: An expression for significant nucleation and model comparison. *Journal of Aerosol Science*, *30*(8), 1079–1094. https://doi.org/10.1016/S0021-8502(98)00776-9

Pyle, D. M., & Mather, T. A. (2003). The importance of volcanic emissions for the global atmospheric mercury cycle. *Atmospheric Environment*, *37*(36), 5115–5124. https://doi.org/10.1016/J.ATMOSENV.2003.07.011

Radke, L. F. (1982). Sulphur and Sulphate from Mt Erebus. *Nature*, *299*, 710–712.

Roberts, T. J., Vignelles, D., Liuzzo, M., Giudice, G., Aiuppa, A., Coltelli, M., et al. (2018). The primary volcanic aerosol emission from Mt Etna: Size-resolved particles with SO2 and role in plume reactive halogen chemistry. *Geochimica et Cosmochimica Acta*, *222*, 74–93. https://doi.org/10.1016/J.GCA.2017.09.040

Robock, A. (2000). Volcanic eruptions and climate. *Reviews of Geophysics*, *38*(2), 191–219. https://doi.org/10.1029/1998RG000054

Rondo, L., Ehrhart, S., Kürten, A., Adamov, A., Bianchi, F., Breitenlechner, M., et al. (2016). Effect of dimethylamine on the gas phase sulfuric acid concentration measured by Chemical Ionization Mass Spectrometry. *Journal of Geophysical Research: Atmospheres*, *121*(6), 3036–3049. https://doi.org/10.1002/2015JD023868

Rose, W. I., & Durant, A. J. (2009). Fine ash content of explosive eruptions. *Journal of Volcanology and Geothermal Research*, *186*(1–2), 32–39. https://doi.org/10.1016/j.jvolgeores.2009.01.010

Rose, W. I., Millard, G. A., Mather, T. A., Hunton, D. E., Anderson, B., Oppenheimer, C., et al. (2006). Atmospheric chemistry of a 33-34 hour old volcanic cloud from Hekla Volcano (Iceland): Insights from direct sampling and the application of chemical box modeling. *Journal of Geophysical Research Atmospheres*,

Accepted Article

111(20), 1–17. https://doi.org/10.1029/2005JD006872

Schmidt, A., Ostro, B., Carslaw, K. S., Wilson, M., Thordarson, T., Mann, G. W., & Simmons, A. J. (2011). Excess mortality in Europe following a future Laki-style Icelandic eruption. *Proceedings of the National Academy of Sciences of the United States of America*, *108*(38), 15710–5. https://doi.org/10.1073/pnas.1108569108

Schmidt, A., Carslaw, K. S., Mann, G. W., Rap, A., Pringle, K. J., Spracklen, D. V., et al. (2012). Importance of tropospheric volcanic aerosol for indirect radiative forcing of climate. *Atmospheric Chemistry and Physics*, *12*(16), 7321–7339. https://doi.org/10.5194/acp-12-7321-2012

Schmidt, A., Leadbetter, S., Theys, N., Carboni, E., Witham, C. S., Stevenson, J. A., et al. (2015). Satellite detection, long-range transport, and air quality impacts of volcanic sulfur dioxide from the 2014-2015 flood lava eruption at Bárðarbunga (Iceland). *Journal of Geophysical Research: Atmospheres*, *120*(18), 9739–9757. https://doi.org/10.1002/2015JD023638

Seidel, D. J., Zhang, Y., Beljaars, A., Golaz, J.-C., Jacobson, A. R., Medeiros, B., et al. (2012). Climatology of the planetary boundary layer over the continental United States and Europe. *J. Geophys. Res*, *117*, 17106. https://doi.org/10.1029/2012JD018143

Sihto, S.-L., Kulmala, M., Kerminen, V.-M., Dal Maso, M., Petäjä, T., Riipinen, I., et al. (2006). Atmospheric sulphuric acid and aerosol formation: implications from atmospheric measurements for nucleation and early growth mechanisms. *Atmospheric Chemistry and Physics*, *6*(12), 4079–4091. https://doi.org/10.5194/acp-6-4079-2006

Simpson, D., Winiwarter, W., Börjesson, G., Cinderby, S., Ferreiro, A., Guenther, A., et al. (1999). Inventorying emissions from nature in Europe. *Journal of Geophysical Research: Atmospheres*, *104*(D7), 8113–8152. https://doi.org/10.1029/98JD02747

Sipilä, M., Berndt, T., Petäjä, T., Brus, D., Vanhanen, J., Stratmann, F., et al. (2010). The role of sulfuric acid in atmospheric nucleation. *Science (New York, N.Y.)*, *327*(5970), 1243–6. https://doi.org/10.1126/science.1180315

Smith, S. J., Van Aardenne, J., Klimont, Z., Andres, R. J., Volke, A., & Delgado Arias, S. (2011). Anthropogenic sulfur dioxide emissions: 1850-2005. *Atmospheric Chemistry and Physics*, *11*(3), 1101–1116. https://doi.org/10.5194/acp-11-1101-2011

Stein, F. A., Draxler, R. R., Rolph, G. D., Stunder, J., Cohen, M. D., & Ngan, F. (2016). NOAA'S HYSPLIT Atmospheric transport and dispersion modeling system. *Journal of Applied Meteorology and Climatology*, *96*(12), 2059–2077. https://doi.org/10.1175/BAMS-D-14-00110.1

Tomasi, C., & Lupi, A. (2016). Primary and Secondary Sources of Atmospheric Aerosol. *Atmospheric Aerosols*, 1–86. https://doi.org/10.1002/9783527336449.ch1

Tulet, P., Muro, A. Di, Colomb, A., Denjean, C., Duflot, V., Arellano, S., et al. (2017). First results of the Piton de la Fournaise STRAP 2015 experiment: multidisciplinary tracking of a volcanic gas and aerosol plume. *Atmos. Chem. Phys*, *17*, 5355–5378. https://doi.org/10.5194/acp-17-5355-2017

Vignelles, D., Roberts, T. J., Carboni, E., Ilyinskaya, E., Pfeffer, M., Dagsson Waldhauserova, P., et al. (2016). Balloon-borne measurement of the aerosol size distribution from an Icelandic flood basalt eruption. *Earth and Planetary Science Letters*, *453*, 252–259. https://doi.org/10.1016/j.epsl.2016.08.027

Volcanology, N. I. of G. and. (2016). *Bollettino settimanale sul monitoraggio vulcanico , geochimico , delle deformazioni del suolo e sismico del vulcano Stromboli, Rep. N° 25/2016*. Retrieved from http://www.ct.ingv.it/en/rapporti/multidisciplinari.html?view=docman&start=195

Watson, I. M., & Oppenheimer, C. (2000). Particle size distributions of Mount Etna's aerosol plume constrained by Sun photometry. *Journal of Geophysical Research Atmospheres*, *105*(D8), 9823–9829. https://doi.org/10.1029/2000JD900042

Weber, K., Eliasson, J., Vogel, A., Fischer, C., Pohl, T., Van Haren, G., et al. (2012). Airborne in-situ investigations of the Eyjafjallajökull volcanic ash plume on Iceland and over north-western Germany with light aircrafts and optical particle counters. https://doi.org/10.1016/j.atmosenv.2011.10.030

Weber, R. J., Marti, J. J., McMurry, P. H., Eisele, F. L., Tanner, D. J., & Jefferson, A. (1996). MEASURED ATMOSPHERIC NEW PARTICLE FORMATION RATES: IMPLICATIONS FOR NUCLEATION MECHANISMS. *Chemical Engineering Communications*, *151*(1), 53–64. https://doi.org/10.1080/00986449608936541

Weber, R. J., Lee, S., Chen, G., Wang, B., Kapustin, V., Moore, K., et al. (2003). New particle formation in anthropogenic plumes advecting from Asia observed during TRACE-P. *Journal of Geophysical Research: Atmospheres*, *108*(D21). https://doi.org/10.1029/2002JD003112

Weigel, R., Hermann, M., Curtius, J., Voigt, C., Walter, S., Böttger, T., et al. (2009). Experimental characterization of the COndensation PArticle counting System for high altitude aircraft-borne application. *Atmospheric*

Accepted Article

Measurement Techniques, *2*(1), 243–258. https://doi.org/10.5194/amt-2-243-2009

Zelenski, M., Taran, Y., & Galle, B. (2015). High emission rate of sulfuric acid from Bezymianny volcano, Kamchatka. *Geophysical Research Letters*, *42*(17), 7005–7013. https://doi.org/10.1002/2015GL065340

Accepted Article